# Multilayer-based Soft X-ray Polarimetry

**Franz Schaefers**

**BESSY, Berlin**

## ABSTRACT

An overview about the soft x-ray polarimetry work done at BESSY over the last 10 years is given. At BESSY ten elliptical undulator beamlines are operating in the VUV and soft x-ray range which enable the polarisation state of the synchrotron radiation to be changed from linear (horizontal or vertical) to left- or right-handed circular. It is essential that the degree of polarisation is quantitatively known, since this is a normalization quantity for many polarisation-sensitive experiments (e.g. MCD-spectroscopy).

For a polarimetry experiment i.e. the measurement of the complete polarisation state of light two optical elements are required acting as phase retarder and as linear polariser, resp. In the soft x-ray range specially tailored multilayers (ML) operating in transmission and in reflection have been developed and optimized for this purpose. By matching the ML-parameters (period, thickness ratio) to an absorption edge of one of the constituent materials a resonantly enhanced polarisation sensitivity can be achieved. Thus, ML-polarimetry is strongly connected with at-wavelength metrology of these polarisation optical elements for which the instrumentation and results are presented.

Examples on magneto-optical spectroscopy and -polarimetry to determine properties of magnetic thin films or optically active substances are also presented (Faraday-, Kerr-effect, L-MOKE).

Another topic which will be covered briefly is the HIgh Kinetic Energy photoelectron spectroscopy (HIKE) employing hard x-rays which recently came up and which is ideally suited to study – sample preserving - deeply buried layers or bulk properties of matter. An example for its application to characterise ML interfaces is shown.

**Keywords:** Multilayer, Soft x-Ray Radiation, EUV, Synchrotron Radiation, Polarisation, Linear Analysers, Phase Plates, Reflectivity, Magneto-Optics

11.04.2007

# 1. Introduction

Studies of magnetic scattering[1,2,3,4] and magneto-optics[5,6,7,8,9] using synchrotron radiation require knowledge of the beam polarization , which is also necessary to characterize EUV optical elements at off-normal incidence angles[10,11,12,13.] The ability to analyze the polarization state of the beam is of practical importance in evaluating the performances of insertion-device synchrotron sources[14]. Experimental control and evaluation of a beam's polarization state can be obtained with optical devices such as phase retarders and linear analyzers[15,16,17.] Periodic MLs are commonly used to study the polarization state of EUV and VUV beams[18,19,20,21,] which must be changed or rotated to perform polarization analyses because of their intrinsically narrow wavelength acceptances. This report gives a review about the polarimetry work done at BESSY, the German storage ring facility during the last two decades.

BESSY operates a medium energy 1.7 GeV storage ring with 16 straight sections of which ten are occupied by soft x-ray Undulators, six of them are elliptical APPLE II-devices for generation of polarised light. More than 40 beamlines are operational from the IR to hard x-rays with special emphasis on the soft x-ray range. Each of the undulators branches the light into two or more beamlines which are useable alternatively. Thus fourteen undulator beamlines and additionally two polarised bending magnet beamlines exploiting the off-plane radiation are dedicated to polarisation sensitive experiments in the EUV, VUV and soft x-ray range[22]. All these beamlines had to be characterised with respect to their polarisation properties.

In chapter 2 this review will briefly discuss the development and characterisation of special ML-optics for polarisation control and steering by the At-Wavelength Metrology. This is a prerequisite for polarisation spectroscopy. Then the ML-polarimetry will be dealt with in chapter 3. In chapter 4 some examples on polarisation spectroscopy are shown, a spin-off from the technique of ML-polarimetry.

## 2. At-Wavelength Metrology


At-Wavelength Metrology is the measure of the performance of an optical element at the wavelength, for which it is designed. Apart from routine tests employing Cu-ka diffractometry which delivers information on interfacial roughness and the quality of the coated reflecting layers and apart from long-trace profilometry which delivers information on the figure and finish errors of optical surfaces the at-wavelength metrology is the most powerful and most essential characterisation tool for the development and characterisation of soft x-ray optics, since the optical properties such as the reflectivity is governed by the optical constants of the materials involved which are strongly dependent on the wavelength.

A dramatic and convincing example for the necessity of at-wavelength metrology as a 'test drive' is shown in the figure 1 [23,24]. This is the reflectivity curve of a Sc/Si ML, which has a Normal-Incidence Bragg reflection at 45 nm, UV-region. The ML with a period thickness of 22.5 nm has only 10 periods, nevertheless it has an extraordinary reflectivity of 50 %. The read curve is obtained by a second ML and this one has a vanishing reflectivity.

The important point here is that the ML are nearly identical, they have been sputtered one after the other in the same chamber under the same conditions. The only difference between them is the outermost layer which is once silicon and once scandium. A Cu-Kα test gives no difference in their performance, which means that their quality, their periodicity and interface perfection is similar, as expected. Such a dramatic effect can be detected only at the design wavelength.

The UV-region is known to be highly absorbing, in other words the penetration depth of the light is rather limited. Thus an optical element is contamination and surface sensitive, because the radiation is absorbed in the outhermost layer - and it is surprising that a ML is performing here at all.


This is due to the anomalous optical features of the Sc absorber material[25]:

Sc as the first element of the 3d-transition metals with electronic configuration $3p^6 3d 4s^2$ has a nearly empty d-shell with just one electron. The 3p-3d electronic transition occurs in the UV-range. Since the d-shell of Sc is nearly unoccupied Sc has the largest oscillator strength of all transition metals connected with largest absorption.

This is connected with an absorption minimum right below the transition which again is most pronounced for Sc. So Sc has the potential of being a good ML absorber material exclusively in this range. The deeper the absorption minimum, the larger is the penetration depth of light.

And the larger the penetration depth - the more layers contribute to the reflection and consequently the larger is the reflectance as can be seen in figure 2, where the reflectivity of different Sc/Si ML is shown. Their period varied systematically to have the Bragg-maximum always at the same angle of $5^o$ to normal.

It is worthwile to mention that at the wavelength of maximum performance, at 46.9 nm, a powerful table-top x-ray laser line is operating[26].

The working range of ML operation in the VUV range is limited to the vicinity of absorption edges of one of the constituent materials. A resonantly enhanced performance increase is thus reachable at the Si-, B-, and C- k edges and for the water window range at the 2p edges of the rare earth elements. However, performance degrades with increasing photon energy, because the material contrast determined by the optical constants reduces strongly and the influence of roughness increases with energy, since the layers approach monolayer thicknesses.

At BESSY a soft x-ray optics beamline for metrology[27] is operational which is coupled to a bending magnet and which is equipped with a reflectometer endstation (figure 3).

This is a collimated Plane Grating Monochromator operating from 20 to 1500 eV. It can be tuned to linear or (off-plane) elliptical polarisation. By operation of the grating in collimated light[28] it has flexibility in the operation modes such as high-order suppression - which is essential for reflectometry.

The most prominent ML for the water window is Cr/Sc to be operated at either the Sc or Cr 2p absorption edges. Their evolution and improvement has been studied over the last decade[29,30]. As shown in the figure 4 we developed two types of reflectors for the Sc-near edge region: Brewster angle mirrors for polarimetry purposes operating close to $45^o$ incidence angle and normal incidence mirrors for water-window microscopy and N-k fluorescence analysis applications.

The reflectivity could be increased by more than a factor of two in both cases and a 20 % normal incidence reflectivity at 400 eV within a 1 eV bandwidth is available today[31].

Such a high-tech mirror requires a sophisticated layer-by layer production and atomic scale interface engineering accompanied by ion assisted deposition. An angular scan which is a depth profile of the ML confirms the high individual layer conformity.

A survey of all the individual reflection data collected over the years is given in the figure 5. Plotted is the peak reflectivity in normal incidence. Each data point corresponds to one individual ML. The resonance behaviour of the reflectivity is clearly seen at all the involved absorption edges up to the Ti and V 2p-edges above 500 eV which seems to be the practical limit for normal incidence spectroscopy. A similar figure can be constructed for the case of Brewster-angle polarisers operating at $45^o$. Since the ML-period in this case is larger by a factor of 1/sin(45) for the same photon energy, polarisers are available at the 2p edges of the magnetic elements Fe, Co and Ni at which most of the polarisation spectroscopy is being performed.

## 3. Multilayer Polarimetry

Multilayer polarimetry is a spin-off from at-wavelength metrology. The detailed knowledge of the polarisation properties of MLs is a prerequisite to its application to the measurement of the complete polarisation state of synchrotron radiation. This is done according to standard optics textbooks, employing two optical elements which are azimuthally rotated around the direction of the light: a polariser to introduce a phase retardation and an analyser for linear polarisation analysis[32].

An ideal polariser retards the phase by a quarter of a wave, and does not act on the amplitude, an ideal analyser suppresses one component completely and does not act on the phase.

Any interaction of the optics with the electromagnetic wave is put into the complex reflection (or transmission) coefficients rs or rp.

$$E_s' = r_s E_s$$
$$E_p' = r_p E_p$$

(1)

The polarisation is described by the Stokes vector, for intensity $S_0$, linear polarisation $S_1$ and $S_2$ and circular polarisation $S_3$.

The interaction process is described by the Mueller matrix

$$M = \begin{bmatrix} 1 & -\cos 2\Psi & 0 & 0 \\ -\cos 2\Psi & 1 & 0 & 0 \\ 0 & 0 & \sin 2\Psi \cos \Delta & \sin 2\Psi \sin \Delta \\ 0 & 0 & -\sin 2\Psi \sin \Delta & \sin 2\Psi \cos \Delta \end{bmatrix}$$

(2)

which is basically determined by two parameters, the ellipticity $\Psi$ and the total phase retardation $\Delta$ to describe the complex reflection or transmission coefficient.

$$\Psi = \text{atan}(r_p/r_s)$$
$$\Delta = \delta_p - \delta_s$$

(3)

So, finally for our two-optical element polarimeter system the Stokes vector at the detector S-final is obtained by the initial Stokes vector of the incoming light, multiplied by the rotation-matrix, mueller-matrix and back rotation matrix of the first optical element (rotated by alpha), and similarly for the second optical element which is rotated by beta[33]:

$$S_{final} = R(-\beta) \, M_2 \, R(\beta) \, R(-\alpha) \, M_1 \, R(\alpha) \, S_{initial}$$

(4)

So the detector sees a 3-D intensity contour such as shown in figure 6 as function of alpha and beta when we assume an ideal polarimeter and circularly polarised incident light S3 = 1 (fig. 6a) and linearly polarised light, respectively (fig. 6b).

A fit of the experimental data to this contour delivers not only the Stokes parameters of the incident light, but also the polarising properties of the optical elements involved such as the *Rs/Rp, Ts/Tp* and the phase shift $\Delta$. Thus this is a self-calibrating measurement, one does not need to know very much about the optics, the measurement itself gives all relevant data. This requires, however, a redundance in the number of measured data and high quality data for the fitting procedure to converge properly.

Linear Analysers and Phase plates are common for the visible, and UV spectral range. In EUV triple- and quadruple-reflection mirrors have been designed with incidence angles for optimum phase retardation or analyser behaviour[34,35]. For the soft x-ray range specially tailored MLs operated in reflection and in transmission have been developed in the last decade[36]. Similarly to the MLs optimised for highest reflection, the phase retardation obtainable with transmission MLs is resonantly enhanced at the absorption edges, thus the tuning range is limited, and the phase shift dies away with higher energies due to roughness and missing contrast in the optical constants.

Several apparatus for full polarisation measurements in the soft x-ray range have been reported[37]. The BESSY soft x-ray polarimeter[20] shown in figure 7 is able to perform such a polarisation measurement according to textbook. In this 6-axis UHV-diffractometer the light hits a polariser and analyser section, both azimuthally rotatable, and the incidence angle is freely changeable. The detector is scanning in the dispersion plane and perpendicular to it.
Up to ten optical elements are selectable from a magazine store in vacuum. Additionally a load-lock system enables rapid sample transfer from air to UHV within half an hour.
This versatility allows the chamber to be used not only as a polarimeter for incident light spectroscopy:
When one of the optics is removed, it is a reflectometer allowing for intensity spectroscopy in transmission or reflection geometry. And for transmitting optics ellipsometry can be done, since not only the transmitted intensity but also the polarisation state after transmission can be studied.
The photo (figure 8) shows a compact version of the polarimeter also in use at BESSY[38]. This one was designed for in-situ control of the polarisation state at various elliptical undulator beamlines, all optical parts are removeable, thus, it can be permanently coupled between the beamline and an experiment.

Figure 9a shows the reflectivity of a Cr/Sc ML obtained for s- and p-polarised light[29]. The period was exactly matched, so that the Bragg-peak coincides with the Brewster angle at $45^{\circ}$ at the design energy, which is close to the Cr 2p edge. The suppression ratio $r_s/r_p$ is more than 1000, thus the polarizing power more than 99.8 %. By such a matching of both polarizing angle and resonance energy the excellent polarizing power is combined with high reflectivity. An azimuthal scan of the polariser around the light direction from 0 to $360^{\circ}$ confirms this behaviour (figure 9b). In normal incidence geometry, however, no angular dependence is observed, as expected. Note, that this ML can be operated in two working ranges: at the Cr edge at $45^{\circ}$ as analyser and at the Sc edge as a highly efficient normal incidence reflector.

Transmission ML-phase plates are sputtered on 120 nm thick $Si_3N_4$ membranes. The Bragg reflection resonance at a certain photon energy manifests itself as transmission minimum at the Bragg-angle. As seen in figure 10a this minimum is resonantly enhanced in the region of the absorption edge - here the Sc 2p edge - and it is connected with a considerable phase retardation as function of the angle in the vicinity of the Bragg-angle (figure 10b).
The measured $30^{\circ}$ phase shift at 400 eV is still far away from a quarter-wave behaviour, but this is sufficient for an unequivocal determination of the polarisation state by the fitting procedure explained above.

A survey about all the phase shift data available are summarised in figure 11. For the UV-range $MgF_2$ optics has been added to this survey and at the Si L edge (100 eV) there is a quarter-wave plate of Mo/Si[18,19]
In the water window range four systems were developed for the C edge and the Sc, Ti and Cr edges. As expected, the performance is strongly dependent on the material combination and it

goes down at higher photon energies. Recently a broad-band Mo/Si ML was reported[3940], which is tuneable in wavelength – in a bandwidth of approximately 10%. This was realised by a random modification of the individual layer thicknesses to make the rocking curve broader - at the price of reflectivity and phase shift.

At the Sc edge a quarter-wave plate was reported recently[21,41] employing high quality Cr/Sc MLs with individual thicknesses in the range of 1 nm. Due to the required ultra-short period the practical limit for this technology has been reached approximately at these energies.

While linear polarisation analysers with sufficient perfection are available at even higher energy[42], it may be worthwile trying to develop phase plates for the magnetic Fe, Co and Ni 2p edges, which require some hundred periods with layer thicknesses down to 0.5 nm, since most of the polarisation spectroscopy work is done here and since no polarisation determination employing optical standards is possible so far. The degree of circular polarisation can be estimated only by transfer standards (such as MCD-detectors[43]) which need to be calibrated once against a linear polarisation standard under the assumption of a complete total polarisation without any unpolarised background radiation.

## 4. Magneto-Optics

Magneto-Optics deals with the interaction of radiation with magnetic materials: the optical response to magnetised matter. In analogy to non-magnetic optics this response is put into magneto-optical constants of the form

$$n_{\pm} = 1 - (\delta_l \pm \Delta\delta) + i\,(\beta_l \pm \Delta\beta) \tag{5}$$

with $\delta_l$ and $\beta_l$ being the non-magnetic optical constants, and $\Delta\delta$ and $\Delta\beta$ the 'magnetic perturbation' of the optical interaction[44]. The positive and negative sign denotes the orientation of the magnetic field with respect to the polarisation direction. The difference $\Delta n = n_+ - n_-$ denotes the circular dicroism of the material. Similarly to the optical interaction, the magneto-optical properties are resonantly enhanced at the absorption edges of the magnetic sub-states, such as the L-, or M-edges of Fe, Co and Ni.

In the BESSY polarimeter chamber (figure 7) samples can be magnetised in-situ by in-vacuum magnetic coils around the sample holder, and an iron yoke close to the sample surface, which directs the magnetic flux through the sample. Two magnetisation directions can be realised each for both the reflection and transmission sample: in-plane in two directions (reflection) and out-of plane (transmission sample). Nevertheless, the full versatility and flexibility in angle settings and in-situ sample change is kept, so that a variety of different measurement techniques could be established, which make use of the many degrees of freedom:
- incident radiation: energy, polarisation
- magnetization direction (in-plane, out-of plane)
- orientation of both light (k-vector and spin) and magnetization: parallel, longitudinal, transversal
- azimuth and incidence angle
- detection channel (intensity, polarisation)

The figure 12 gives an overview about this zoo of experimental possibilities connected with magneto-optical effects[45]. They can first be classified according to the detection channel, whether the intensity or the polarisation of the scattered light is being investigated after the interaction process. The magnetic sensitivity is either linear or quadratically with the magnetic field. An effect linear in M changes sign on magnetisation reversal, an odd effect does not.
Some effects are proportional to the degree of circular polarisation, others to the degree of linear polarisation, while the other Stokes component in this case is ineffective.

For instance, the classical MCD probes the spin-up and spin-down bands, so it is measurable with circularly polarised light and the magnetic contrast, the asymmetry is obtained by reversing the orientation (parallel - antiparallel) between magnetization direction and photon helicity.
The linear dicroism is measured in a different geometry, since it is a $M^2$ effect, the contrast is given by parallel and perpendicular orientation between electric field vector and magnetization.
Polarisation spectroscopy with MLs enables the classical Faraday effect (transmitting samples) and Kerr effect - L-MOKE (in reflection) to be measured resonantly enhanced by tuning the photon energy to the 2p-absorption edges in the soft x-ray range. These effects are linear in M, thus change sign on M-reversal and have the advantage that their measurement requires linearly polarised light only, which usually is easier to obtain rather than circular polarisation.

An example for the measurement of the Faraday effect is given in figure 12 [4647]. Here a polarisation measurement of the incident light (black curve) and the light after transmission through a magnetised Fe-film (red curve) is shown. After transmission the polarisation plane is tilted and an ellipticity is induced. Both ellipsometric parameters $\phi$ and $\tan\varepsilon$ can be traced back to the magneto-optical quantities $\Delta\delta$ and $\Delta\beta$

The Faraday-rotation angles are 100 times larger than measured in the visible, when it is measured element-specific and resonantly enhanced within the 2p-absorption edge.

Such a thin magnetic film can be used for steering of the linear polarisation plane - to rotate the e-vector by up to $90^{\circ}$, the angle is determined by the thickness of the film.

Though the Faraday-effect is measured with linearly polarised light, the dicroism is sampled with this technique, since the linear polarisation can be though of being composed by two circular polarised waves of equal intensity, but opposite helicity, of which the absorption is different due to the circular dicroism of the system.

For polarisation spectroscopy to be established as a tool for magnetic materials research the transmission geometry is of rather limited use, since most samples cannot be thinned down to ultra-thin films of less than a nanometer to have significant transmitted signal. The analogon to the Faraday-effect in reflection is called Kerr-effect, i.e. the polarisation analysis of the light reflected by a magnetic sample. By an additional miniaturised polarisation detector sitting on the detector holder such a measurement is possible using the BESSY polarimeter.

Figure 13 gives an example for the Kerr-effect measured on a Co sample using linearly polarised light[48]. The reflectivity and the change of polarisation in terms of rotation angle $\phi$ and ellipticity $\tan\varepsilon$ was measured across the Co 2p absorption. Both data are used for determination of the magneto-optical constants according to:

$$Rotation \qquad \theta_s = \frac{\Delta\delta(\beta_1 - \beta_o) - \Delta\beta(\delta_o - \delta_1)}{(\delta_o - \delta_1)^2 - (\beta_1 - \beta_o)^2}$$

$$Ellipticity \qquad \varepsilon_s = \frac{\Delta\delta(\delta_o - \delta_1) - \Delta\beta(\beta_1 - \beta_o)}{(\delta_o - \delta_1)^2 - (\beta_1 - \beta_o)^2}$$

$$(6)$$

the indexes 0 and 1 correspond to vacuum level (or a non-magnetic top-layer) and to the non-magnetic part of the refractive index (see eq. 5), respectively. The agreement with data obtained by other methods like MCD and resonant Bragg-reflection is good.

This technique of polarisation spectroscopy which is nothing but soft x-ray ellipsometry is not restricted to magnetic samples and to magnetic dicroism. All optically active samples, which have intrinsically any kind of anisotropy can be addressed element-specifically.

The figure 14 shows the experimental data for a graphitic sample[49]. Graphite has a hexagonal crystal structure - and this structural anisotropy leads to a natural linear dicroism. It is strongly birefringent at the Carbon k-edge. The incident linear polarisation is resonantly modified within the absorption resonance. The polarisation plane is rotated by up to $90^{\circ}$ and also a circular polarisation is induced.

Such a behaviour has serious consequences for optical elements inside a synchrotron radiation beamline, where typically carbon contamination is encountered due to the heat loading on the mirror surfaces. Regardless of the chemical composition of the carbon layer the beamline will be optically active! Not only the photon flux drops at the carbon edge, the polarisation

changes dramatically! Thus polarisation sensitive experiments at the carbon edge need a careful monitoring of the polarisation stage.

## 6. Conclusions

The interaction of polarised soft x-ray radiation with matter can best be studied by polarisation spectroscopy. This allows for the determination of the complex optical constants. By selecting the photon energy this technique is element specific and by tuning the incidence angle it is depth selective.

It is suited for the investigation of e.g. optically active substances – by which a symmetry break in the reaction geometry is induced by any kind of anisotropy such as natural birefringence or magnetic-field induced dicroism.

To measure all this requires polarisation sensitive optical elements for polarisation steering and control. They work best – resonantly enhanced - at their respective absorption edges. Therefore an indispensable tool for their characterisation and development is the at-wavelength metrology.
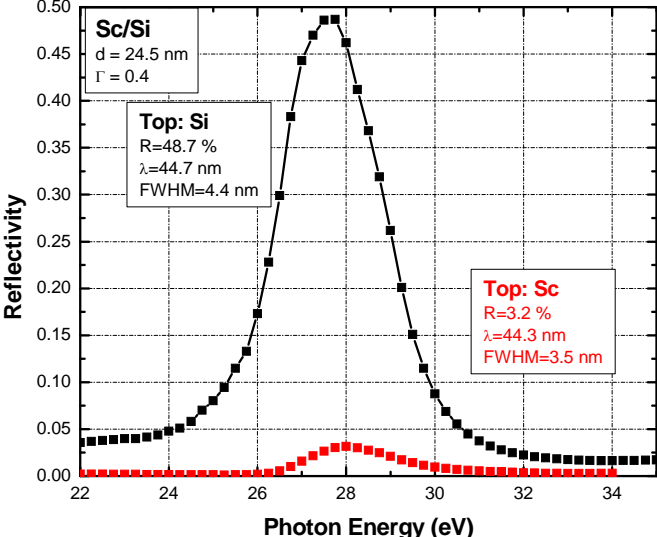
# Figures



**Figure 1**  Comparison of two similar Sc/Si multilayers with Si (black) and Sc (red) top layer coating measured 'at wavelength'
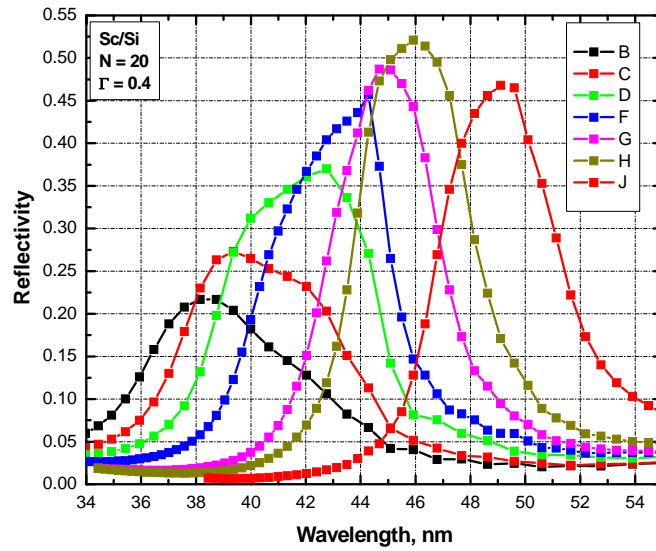
**Figure 2** Normal-Incidence reflectivity (θ=85°) of Sc/Si multilayers with different periods measured in the UV range
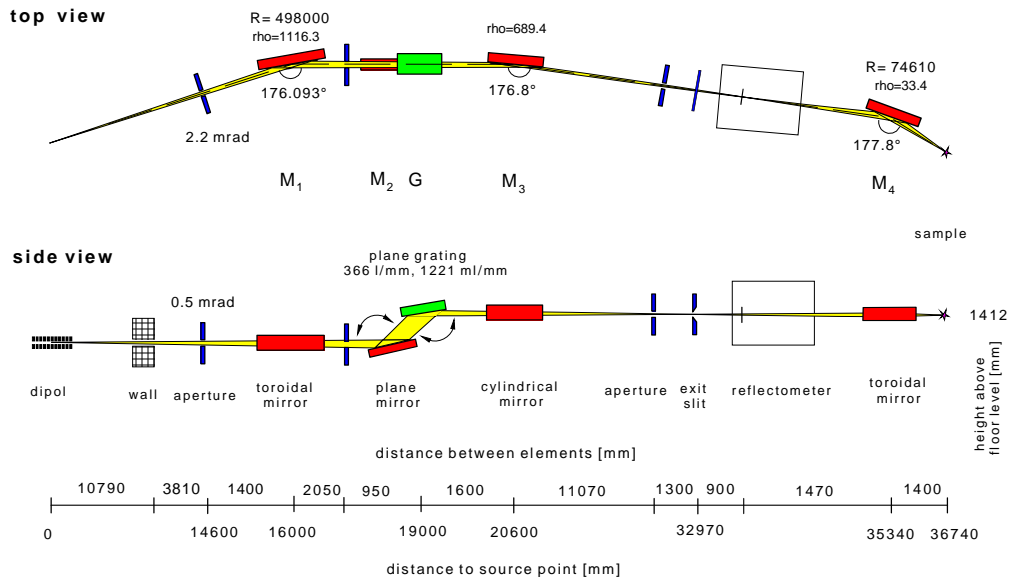
**Figure 3** The BESSY soft x-ray optics beamline for at-wavelength metrology of optical components employing a plane grating monochromator in collimated light
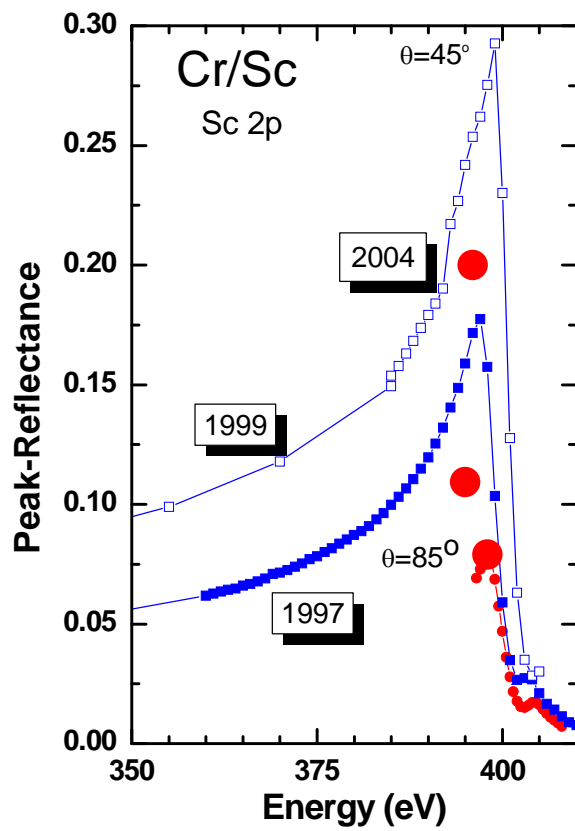
**Figure 4** Evolution of Cr/Sc reflectivity in the water window during the last decade. Normal incidence (red) and Brewster angle (blue)
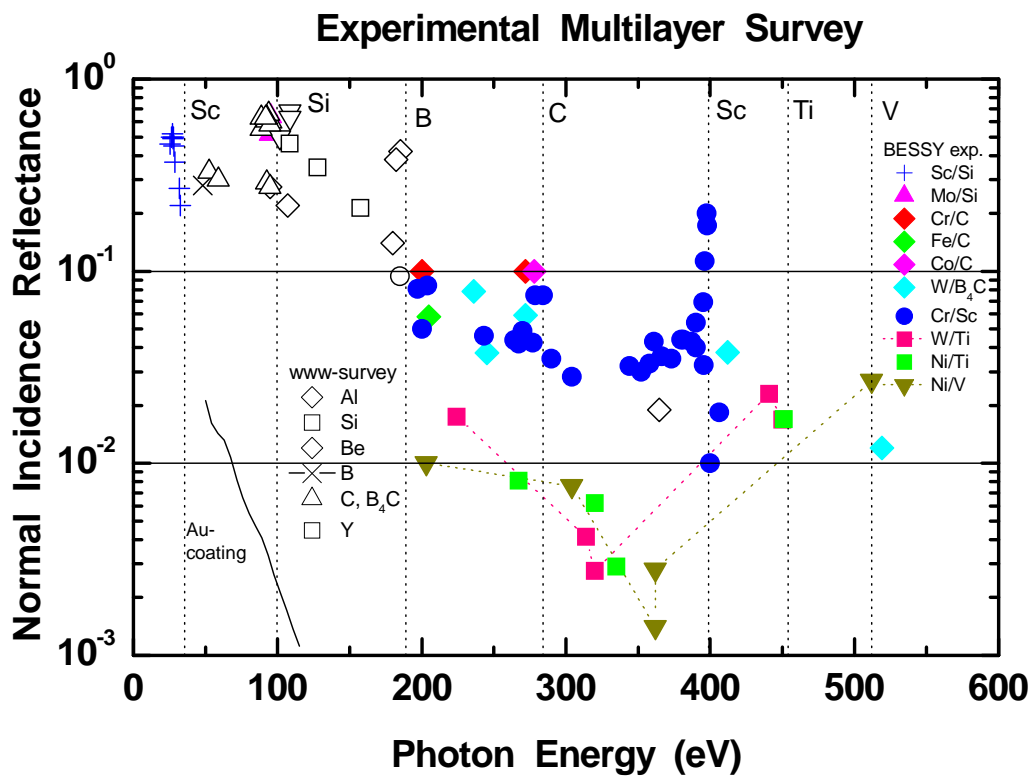
**Figure 5** Experimental Multilayer Survey for the UV, EUV and soft x-ray range. Normal incidence reflectivity is shown only ($\theta > 80^{\circ}$)

**6a**
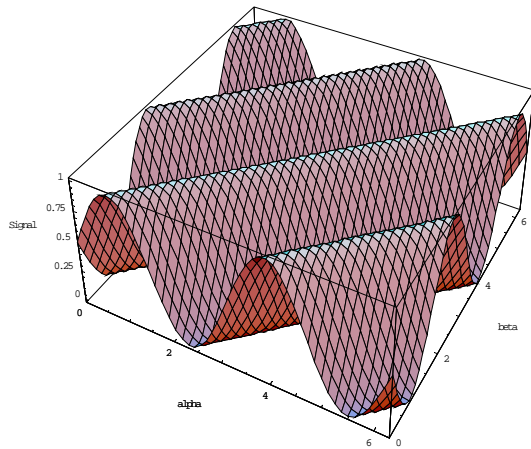
**6b**
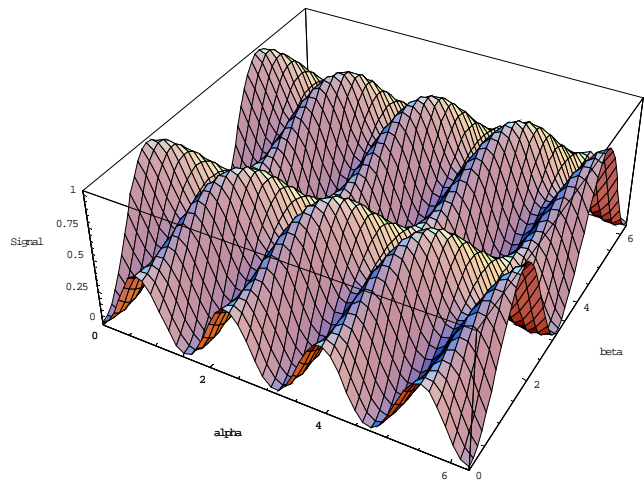


**Figure 6** Calculated Polarimeter signal for circularly (Fig. 6a) and linearly polarised (Fig. 6b) light assuming an ideal polarimeter optics ($T_s=T_p$, $\Delta=90^o$, $R_p=0$)
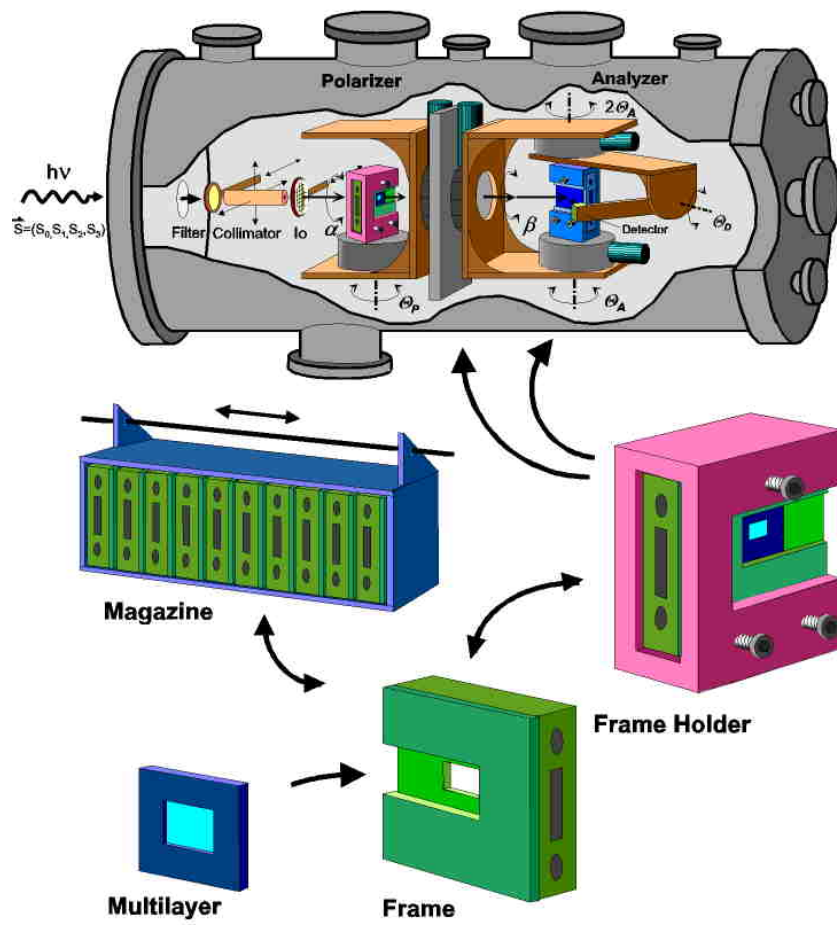
**Figure 7** The BESSY soft x-ray UHV-compatible 6 axis Polarimeter
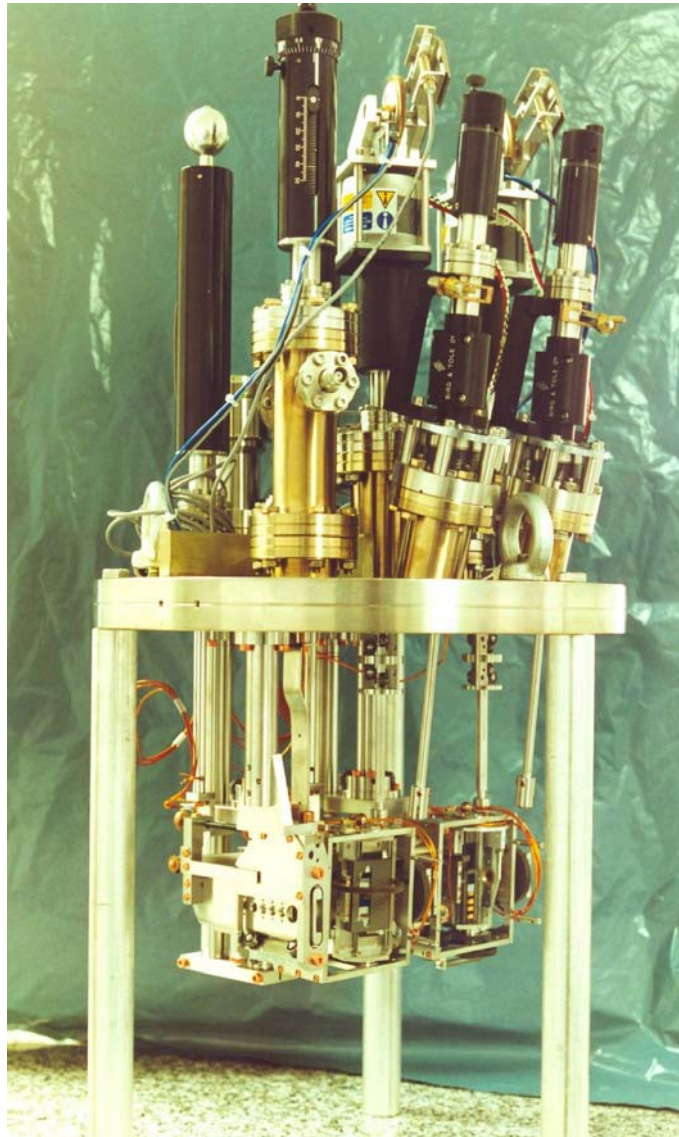
**Figure 8**  The BESSY compact polarimeter for in-situ control of polarisation with removeable optics
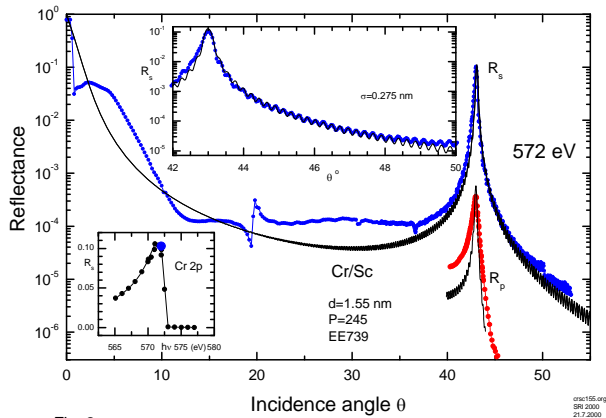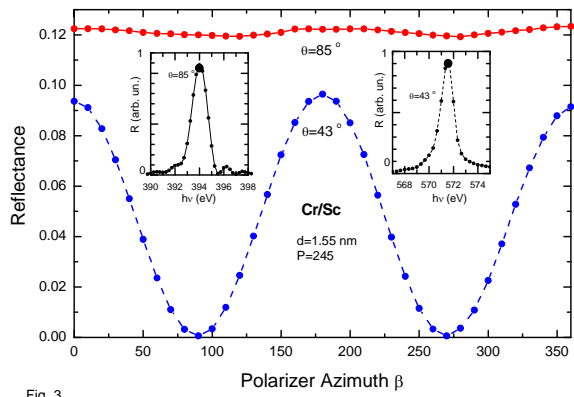
**Figure 9a** Reflectivity of Cr/Sc ML for s- and p-polarised light at 572 eV, right below the Cr 2p absorption edge (see inset). The range of the Brewster angle is enlarged in the inset.

**Figure 9b** Polarimeter scans at the Brewster angle (blue) and in normal incidence, respectively. The energies correspond to Cr and Sc absorption edges, respectively (see inset).
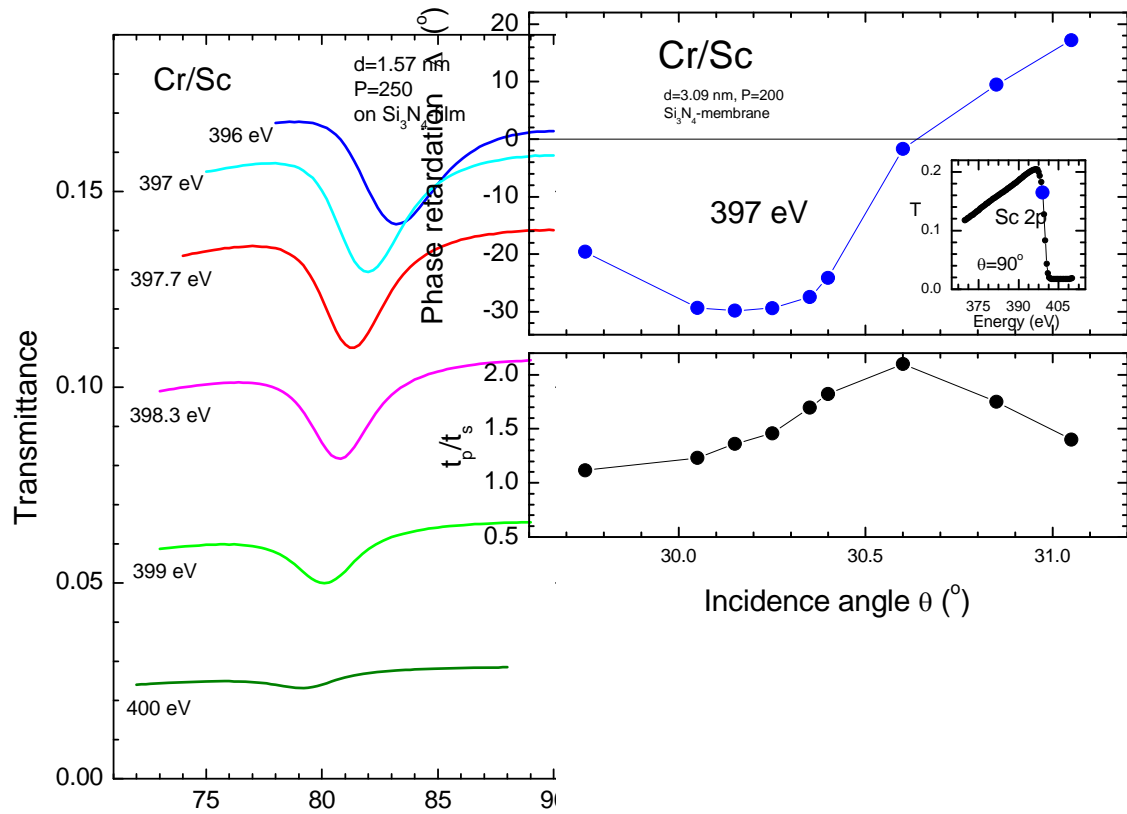
**Figure 10a** Transmission of a Cr/Sc ML on a SiN membrane in the vicinity of the Sc 2p resonance.

**Figure 10b** Corresponding Phase retardation through the Bragg transmission minimum.

**Figure 11**  Survey of Magneto-Optical effects and their measurement
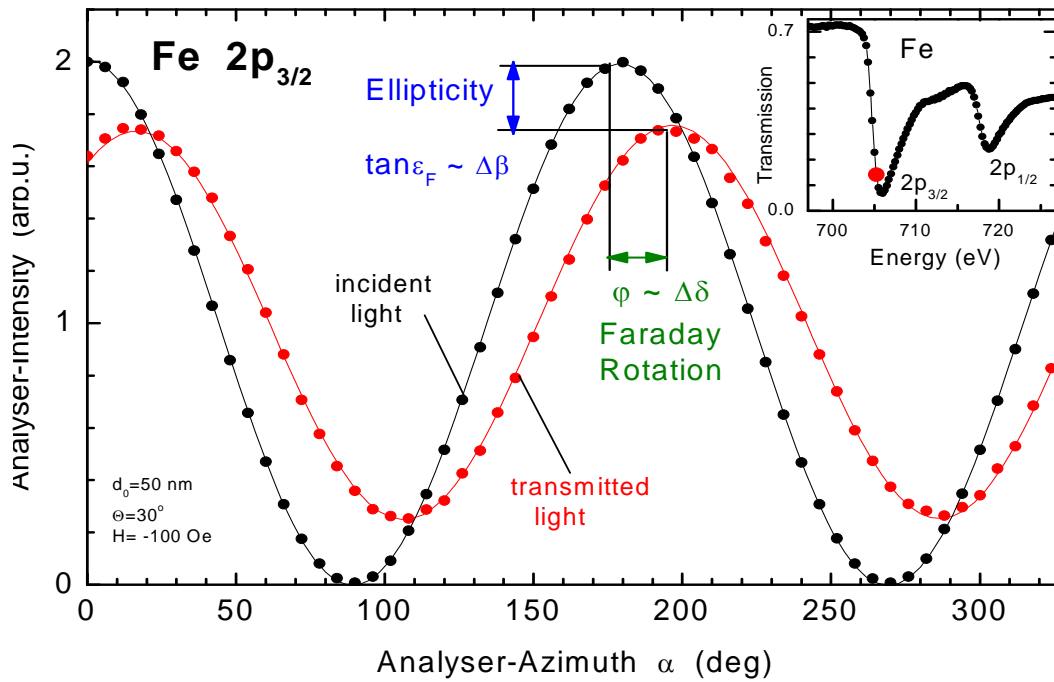
**Figure 12** Ellipsometry on magnetic Fe: Faraday effect on a thin Fe film measured with linearly polarised light resonantly enhanced within the Fe 2p absorption edge (see inset)
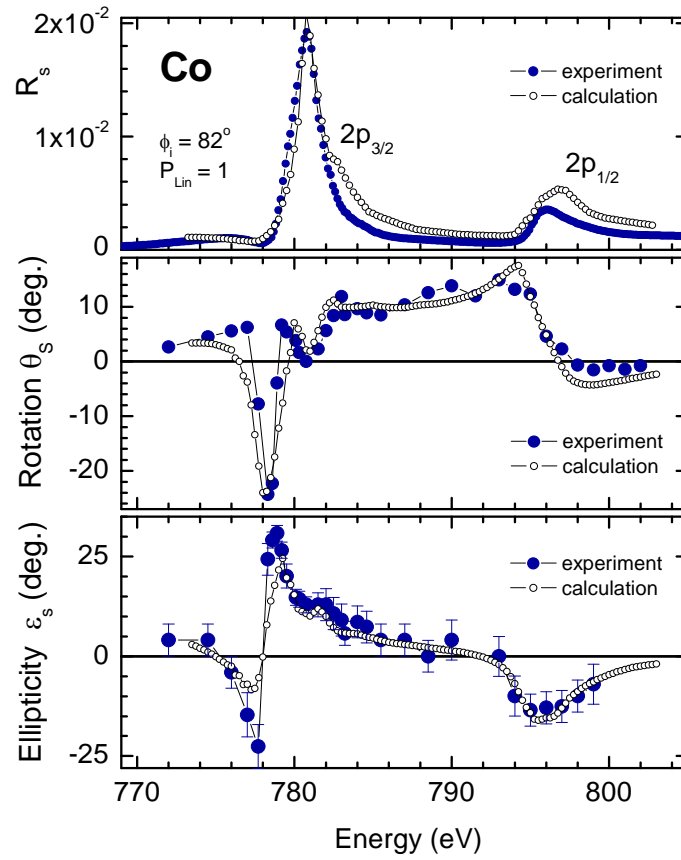
**Figure 13** Ellipsometry on magnetic Co: Kerr effect on a thin Co film measured with linearly polarised light resonantly enhanced across the Co 2p absorption edge
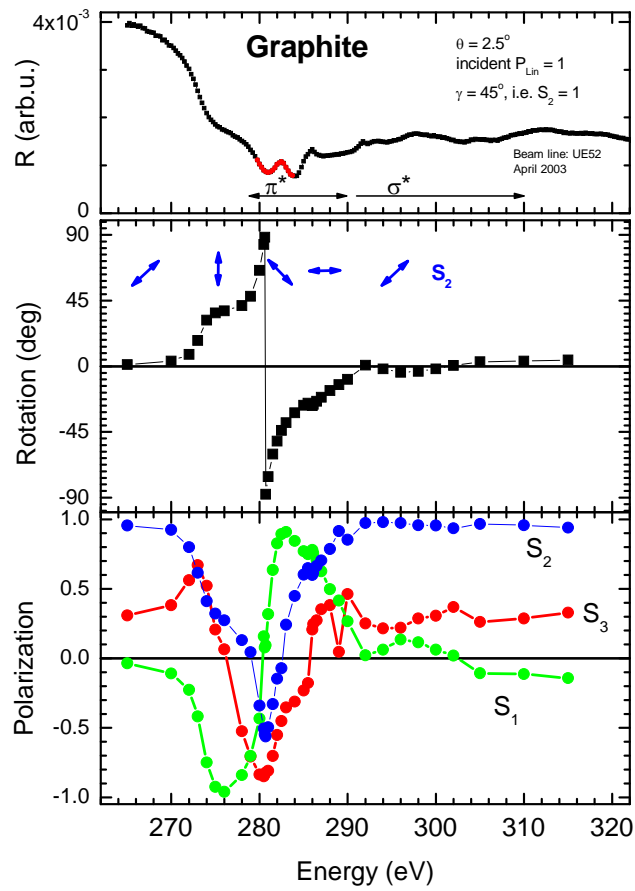
**Figure 14** Ellipsometry on a dicroic graphitic Carbon : Kerr effect on a hexagonal graphite crystal measured with linearly polarised light resonantly enhanced across the C 1s absorption edge

# References

1 M. Hecker, S. Valencia, P.M. Oppeneer, H.-Ch. Mertins,C.M. Schneider, *Phys.Rev. B*, **72**, 054437 (2005))

2 J. B. Kortright, D. D. Awschalom, J. Sto¨hr, S. D. Bader, Y. U. Idzerda, S. S. P. Parkin, I. K. Schuller, and H.-C. Siegmann, J. Magn. Magn. Mater. **207**, 7 (1999)

3 J. B. Kortright and S. K. Kim, Phys. Rev. B **62**, 12 216 (2000)

4 H. A. Duerr, E. Dudzik, S. S. Dhesi, J. B. Goedkoop, G. van der Laan, M. Belakhovsky, C. Moduta, A. Marty, and Y. Samson, Science **284**, 2166 (1999)

5 C. C. Kao, C. T. Chen, E. D. Johnson, J. B. Hastings, H. J. Lin, G. H. Ho, G. Meigs, J.-M. Brot, S. L. Hulbert, Y. U. Idzerda, and C. Vettier, Phys. Rev. B **50**, 9599 (1994)

6 J. Geissler, E. Goering, M. Justen, F. Weigand, G. Schuetz, J. Langer, D. Schmitz, H. Maletta, and R. Mattheis, Phys. Rev. B **65**, 020405 (2001)

7 M. Sacchi and A. Mirone, Phys. Rev. B **57**, 8408 (1998)

8 H.-Ch. Mertins, P. M. Oppeneer, J. Kunes, A. Gaupp, D. Abramsohn, and F. Schaefers, Phys. Rev. Lett. **87**, 047401 (2001)

9 H.-Ch. Mertins, D. Abramsohn, A. Gaupp, F. Schaefers, W. Gudat, O. Zaharko, H. Grimmer, P.M. Oppeneer, Phys. Rev. B **66**, 184404/1-8 (2002)

10 F. Schaefers, Physica B **283,** 119-124 (2000)

11 S.S. Andreev, A.D. Akhsakhalyan, M.A. Bibishkin, N.I. Chkhalo, S.V. Gaponov, S.A. Gusev, E.B. Kluenkov, K.A. Prokhorov, N.N. Salashchenko, F. Schaefers, S.Yu. Zev, Central European Journal of Physics, CEJP **1** 191-209 (2003)

12 H. Grimmer, P. Böni, U. Breitmeier, D. Clemens, M. Horisberger, H.-Ch. Mertins, F. Schaefers, Thin Solid Films **319,** 73-77 (1998)

13 C. Montcolm, P.A. Kearney, J.M. Slaughter, B.T. Sullivan, M. Chaker, H. Pepin, C.M. Falco, Appl. Optics **35**, 5134-5147 (1996)

14 M.R. Weiss, R. Follath, K.J.S. Sawhney, F. Senf, J. Bahrdt, W. Frentrup, A. Gaupp, S. Sasaki, M. Scheer, H.-Ch. Mertins, D. Abramsohn, F. Schaefers, W. Kuch, W. Mahler, Nucl. Instrum. Meth. in Phys. Res, **A467-8**, 449-452 (2001)

15 M.V. Klein, T.E. Furtak, *Optik,* Springer-Lehrbuch (1988)

16 M. Born and E. Wolf, *Principles of Optics*, 6th ed., Pergamon Press (1980)

17 F. A. Jenkins and H.E. White, *Fundamentals of Optics*, 4th ed., McGraw-Hill (1981)

18 J.B. Kortright, J.H. Underwood, Nucl. Instrum. Meth. **A291,** 272-277 (1990)

19 J.B. Kortright, Proc. SPIE **2010**, 160-167 (1993)

20 F. Schaefers, H.-Ch. Mertins, A. Gaupp, W. Gudat, M. Mertin, I. Packe, F. Schmolla, S. DiFonzo, G. Soullie, W. Jark, R.P. Walker, X. Le Cann, R. Nyholm, M. Eriksson, Applied Optics **38**, 4074-4088 (1999)

21 H. Kimura, T. Hirono, Y. Tamenori, Y. Saitoh, N.N. Salashchenko, T. Ishikawa, J. Electron Spectr. and relat. Phenom. **144-147,** 1079-1091 (2005)

22 J. Bahrdt, W. Fentrup, A. Gaupp, M. Scheer, W. Gudat, G. Ingold, and S. Sasaki, Nucl. Instrum. Methods A **467-468,** 21–29 (2001)

23 F. Schaefers, S. Yulin, T. Feigl, N. Kaiser, SPIE-Proc. Vol. **5188**, 138-145 (2003)

24 S. Yulin, F. Schaefers, T. Feigl, N. Kaiser, SPIE-Proc. Vol**. 5193,** 155-163 (2003)

25 A.V. Vinogradov, Quantum electronics **32,** 1113-1121 (2002)

26 B.R. Benware, C.D. Macchietto, C.H. Moreno, J.J. Rocca, Phys. Rev. Lett., **81**, 5804 (1998)

27 http://www.bessy.de/users_info/02.beamlines/

28 R. Follath, Nucl. Instrum. and Methods **A 467**: 418-425 Part 1 (2001)

29  F. Schaefers, H.-Ch. Mertins, F. Schmolla, I. Packe, N.N. Salashchenko, E.A. Shamov, Applied Optics **37**, 719-728 (1998)

30  F. Schaefers, M. Mertin, D. Abramsohn, A. Gaupp, H.-Ch. Mertins, N.N. Salashchenko, S.S. Andreev, Nucl. Instrum. Meth. in Phys. Res. A**467-8**, 349-353 (2001)

31  J. Birch F. Eriksson, F. Schaefers, E.M. Gullikson, S. Aouadi, N. Ghafoor, S. Rohde, L. Hultman, J. Birch, Applied Optics, submitted (2005)

32  W.B. Westerveld, K. Becker, P.W. Zetner, J.J. Corr and J.W. McConkey, Appl. Opt. **24**, 2256-2262 (1985)

33  A. Gaupp, M. Mast, Rev. Sci. Instrum. **60**, 2213-2215 (1989)

34  A. Gaupp, W. Peatman, Proc. SPIE **733**, 272-273 (1986)

35  L. Nahon, Ch. Alcaraz, Appl. Opt. **43**, 1024-37 (2004)

36  H. Grimmer, O. Zaharko, H.-Ch. Mertins, F. Schaefers, Nucl. Instrum. Meth. in Phys. Res. **A467-8**, 354-357 (2001)

37  H. Kimura, T. Hirono, T. Miyahara, M. Yamamoto, T. Ishikawa, Proc. SRI AIP 537-540 (2004)

38  H.-Ch. Mertins, F. Schaefers, D. Abramsohn, A. Gaupp, W. Gudat, E. Meltchakov, S. DiFonzo, W. Jark, O. Zaharko, H. Grimmer, BESSY annual report, 342-343 (2000)

39  Z. Wang, H. Wang, J. Zhu, Z. Zhang, Y. Xu, S. Zhang, W. Wu, F. Wang, B. Wang, L. Liu, L. Chen, A.G. Michette, S.J. Pfauntsch, A K. Powell, F. Schaefers, A. Gaupp, M. MacDonald, Appl. Phys. Lett. **90(3)** 031901 (2007)

40  Z. Wang, H. Wang, Z. Zhang, J. Zhu, S. Zhang, F. Wang, W. Wu, L. Chen, A.G Michette, S.J Pfauntsch, A.K. Powell, F. Schaefers, A. Gaupp, M. Cui, L. Sun, J. Zhu, M. MacDonald, Appl. Phys. Lett., in press (2007)

41  T. Hirono, H. Kimura, T. Muro, Y. Saitoh, T. Ishikawa, J. Electr. Spectrosc. and relat. Phenom. **144-147**, 1097-1099 (2005)

42  A. Gaupp, F. Schaefers, St. Braun, BESSY Annual Report, p. 449-450 (2005)

43  K. Holldack, F. Schaefers, T. Kachel, and I. Packe, Rev. Sci. Instrum. **67**, 2485 (1996)

44  P.M. Oppeneer: in *Handbook of Magnetic Materials,* Vol. **13,** ed. by K.H.J. Buschow (Elsevier, Amsterdam 2001) pp. 229-422

45  H.-Ch. Mertins, S. Valencia, A. Gaupp, W. Gudat, P.M. Oppeneer, C.M. Schneider, Appl. Phys. **A80**, 1011-1020 (2005)

46  H.-Ch. Mertins, F. Schaefers, X. LeCann, A. Gaupp, W. Gudat, Phys. Rev. **B61**, R874-7 (2000)

47  J.B. Kortright, S.K. Kim, Phys. Rev **B62**, 12216 (2000)

48  H.-Ch. Mertins, S. Valencia, D. Abramsohn, A. Gaupp, W. Gudat, P. Oppeneer, Phys. Rev. **B69**, 064407 (2004)

49  H.-Ch. Mertins, P.M. Oppeneer, S. Valencia, W. Gudat, F. Senf, P.R. Bressler, Phys. Rev. **B70**, 235106 (2004)